JEE Journal of Ecological Engineering

Journal of Ecological Engineering 2024, 25(3), 38–52
https://doi.org/10.12911/22998993/177628
ISSN 2299–8993, License CC-BY 4.0

Received: 2023.12.01
Accepted: 2023.12.27
Published: 2024.01.22

Isothermal and Kinetics Investigation of Dibenzothiophene Removal from Model Fuel by Activated Carbon Developed from Mixed Date Seed and PET Wastes

Hajir N. Saeed[1*], Abdelrahman B. Fadhil[1], Omar A Shareef[1]

[1] College of Science, Department of Chemistry, Mosul University, Majmoaa Street, 41002, Mosul, Iraq

* Corresponding author's e-mail: abdelrahmanbasil@yahoo.com

ABSTRACT

This study focuses on the synthesis of activated carbon (AC) using a mix of polyethylene terephthalate (PET), and date seeds (DS) by the optimized $ZnCl_2$-activation method for the first time. At 600 °C for 1 h utilizing an impregnation ratio of 2:1 $ZnCl_2$: mix, the ideal AC was synthesized. The latter was submitted to identification by N_2 adsorption-desorption isotherms and pore volume, XRD, FESEM, EDX, total basic and acid groups, FTIR, and pH_{PZC}, and the outcome suggested its mesoporous structure with an average pore size of 3.16 nm and a BET surface area of 672.22 m^2/g. This AC was tried in the dispose of dibenzothiophene (DBT) from model oil (DBT/n-hexane), and the findings showed that the superlative elimination of DBT (95.07%) was accomplished at 35 °C for 80 min using 0.30 g of the AC. Eliminating DBT by the AC derived from the said mix was best represented by the Langmuir adsorption isotherm and pseudo-2nd-order kinetics model. An adsorptive capacity of 23.80 mg/g was obtained as per the Langmuir adsorption isotherm.The regenerated AC demonstrated an outstanding adsorptive performance for DBT up to 4 cycles of reuse, signifying its high adsorption performance.

Keywords: mixed solid wastes, activated carbon, adsorptive desulfurization, adsorption isotherms and kinetics.

INTRODUCTION

Adsorption has proven its efficiency in eliminating multiple contaminants from various liquid phases. Due to their harmful effects on the environment, the emission of sulfur oxides (SO_x) originated by the combustion of fuel containing S-compounds, desulfurization of fossil fuels verified its importance in petroleum refineries(Sadare and Daramola., 2019). The SO_x react with atmospheric moisture to create acidic rain, which affects vegetation along with aquatic, animal, and human life (Saleh et al., 2018). Both the EU and US have imposed strict limits on the amount of organosulfur compounds (OSC) level in fuels to be between 10 and 15 ppm (Moosavi and Karimzadeh, 2015). For this reason, intense interest has been given to find out reliable methods to lessen the content of the OSC, namely thiophene (T), benzothiophene (BT), and dibenzothiophene (DBT) from transportation fuels (gasoline and diesel fuel) (Saleh., 2020). Hydrodesulfurization (HDS) is commonly employed as the standard process in desulfurizing fuels in refineries. Nevertheless, the need to high temperatures, pressure, and hydrogen intake, are the essential drawbacks of this route(Saleh., 2020; Raut et al., 2022). As such, alternative methods for replacing or supplementing HDS have been investigated, including biodesulfurization (BDS), extractive desulfurization (EDS), adsorptive desulfurization (ADS), and oxidative desulfurization (ODS) (Dehghan and Anbia., 2017; Ganiyu and Lateef., 2021). Among the aforementioned routes, the ADS is one of the most cost-effective and eco-friendly approaches for eliminating OSC from liquid fuels. This process is characterized by their simple operating conditions (lower temperatures and pressures) and the affordability of cheap and regenerable sorbent materials. Also, most of the adsorbents can be easily regenerated, either through thermal

processes or solvent washing (Yaseen et al.,2021; de la Cruz et al., 2020). To date, multiple adsorbents were applied in the ADS, like metal–organic frameworks (An., 2018), carbon materials (Saleh et al., 2018; Mohammed-Taib and Fadhil., 2021; Alhamed and Bamufleh, 2009), metal oxides (Hou et al., 2018), clays (Ali., 2018), and zeolites (Song et al., 2013). Among the carbon derived materials that was widely implemented in the ADS process is the AC as an outcome of its elevated surface area besides its surface, which owns multiple effective functional groups, which take part in the ADS processes. Also, AC has multiple pores with various dimensions, which enhance the removal ability to OSC from fuel oils (Danmaliki and Saleh, 2016; Hussein and Fadhil, 2021). The commercial AC samples are limited in their use due to the expensive cost of their raw precursors along with regeneration and reactivation methods. As such, bio-wastes and synthetic wastes were widely employed in the manufacture of AC. Numerous biowastes, including date stones (DS) (Alhamed and Bamufleh, 2009), olive stones (Deng et al., 2023), sugarcane bagasse (Tao et al., 2015), coconut shells (Keppetipola et al., 2021), etc. were exploited as cheap sources in synthesizing AC. On the other hand, synthetic wastes, such as waste tires rubber (Saleh et al., 2018; Danmaliki and Saleh., 2016), polyethylene terephthalate wastes (Varila et al., 2017), waste polyurethane (Arslanoğlu et al., 2020), etc., were also implemented in the creation of AC. Two main approach were implemented in preparing AC viz. the physical activation, which involves the carbonization or pyrolysis of raw precursor to strip H and O from the chemical composition of the pristine feed, followed by activating the resultant char at elevated temperatures under a flow of steam, N_2, air, or CO_2 (Ahmed and Theydan, 2015). The second rout is the chemical activation, which can be accomplished via impregnating the precursor with multiple chemical agents, like KOH, NaOH, H_3PO_4, H_2SO_4, $ZnCl_2$, etc., followed by pyrolysis and activation in a single-step at temperatures below those required for the physical activation (An et al., 2018). The production of AC from different precursors to be then implemented in the dispose of many S-compounds, including DBT from numerous liquid fuel was announced in the literature. The dispose of DBT from model gasoline by the *Eupatorium adenophorum* derived AC, was examined by Wang et al. (2014). A binary blend of DS and olive stones was transformed to AC to be applied later in eradicating DBT from model liquid fuel (Hussein and Fadhil, 2021). The conversion of sewage sludge as well as corn straw into AC using the activation method with KOH was tried by Zeng et al. (2018), and the prepared AC was employed in H_2S elimination. Lastly, Fadhil and Kareem (2021) explored the ADS of model gasoline employing the $ZnCl_2$-activated biochar created from a mix of DS and olive stones. Eliminating the OSC from diverse fuel oils using the AC originated from DS was touched in the literature, as reported by Alhamed and Bamufleh (2009) and by Bamufleh (2009). Those authors prepared AC from the DS via the $ZnCl_2$-activation approach, and implementing the resultant AC in removing DBT from model diesel. Owing to the widespread use of polymers, the amount of waste generated globally from polymers reached approximately 353 and 369 Mt in 2019 and 2021, respectively. This amount is expected to increase significantly over the next several decades, reaching 1014 Mt in 2060 (Demiral et al 2016). Polymer wastes are now managed mostly through incineration, landfills, combustion, chemical recycling, and mismanagement (Wu et al., 2023). Approximately half of the world's polymer wastes, are disposed of in landfills, with the remaining 19% going by incineration. Nonetheless, globally, only approximately 9% of garbage is recycled. Polymeric wastes own the potential to be consumed by many creatures and build up in the ecosystem, endangering the environment and public health (Demiral et al., 2016; Wu et al., 2023). On the other hand, discarding bio-wastes, like DS into the environment will also be associated with several eco-issues, and thus threatening the environment and public health (Fadhil and Kareem, 2021). Many methods were proposed for getting rid of various solid wastes (waste polymers and waste biomass). Among these methods are the thermochemical processes, like pyrolysis and gasification. Thermal pyrolysis aims to convert such organic wastes into liquid, solid, and gaseous products. On the other hand, gasification is used to convert such wastes into H_2 gas and syngas (Fadhil and Kareem, 2021). Nevertheless, as such wastes can be considered as significant carbon precursors, they were implemented in the production value-added carbonaceous materials, such as the AC (Saleh et al., 2018; Fadhil and Kareem, 2021; Alhamed and Bamufleh, 2009). Thus, after reviewing the literature, we found no

work on the exploiting of an equal mix of solid wastes viz. the DS and PET in creating new AC via the optimized $ZnCl_2$-activation method. Additionally, to the best of our knowledge, the application of the resulting AC for extracting DBT from model fuel has not yet been established.

Herein, the $ZnCl_2$-activation approach was implemented to create AC from an analogous blend of DS and PET. After identifying the AC by many techniques, the ADS of model fuel by this AC was tried with optimizing the process parameters. The adsorption kinetics and isotherms of DBT adsorption by this AC was carried out as well. Finally, reusability of the consumed AC was also adopted.

EXPERIMENTAL

Materials and methods

The source of PET used in this work, was the waste water bottles. The palm date fruit was brought form local markets, and the DS were detached from the fruit. n-Hexane (99.0%), Dibenzothiophene (DBT), NaOH (granulated, 98.0%), HCl (37%), $ZnCl_2$ (97.0–100.50%), $Na_2S_2O_3 \cdot 5H_2O$ (99.0–100.5%,), and I_2 solution (0.1 N), were bought from Scharlau chemicals, Spain. Chemicals and reagents implemented here, were of analytical reagent (AR) grade.

Preparation of AC from mixed DS+PET

The PET bottles were rinsed with water to remove any dirt, and then shredded into little pieces (0.5 cm). Meanwhile, the DS were extensively washed with DW to strip any unwanted contaminants, oven-dried at 105 °C for 5 h, followed by crushing and sieving to attain particles of 0.25 mm size. Creating the AC was accomplished using an equal mixture of DS and PET employing the $ZnCl_2$-activation route. The said blend of waste was mixed with aqueous solutions of $ZnCl_2$ having various impregnation ratios (IR, 0.5–1: 3:1). The mixture was homogenized for 5 h at 300 rpm with a magnetic stirrer. Water was stripped from the blend by drying at 105 °C. A vertical furnace was employed in activating the samples at 400–800 ºC, 10 ºC/min rate of heating for a period between 30 to 120 min. After activation, the activated samples were soaked in 10% HCl, rinsed with hot DW until neutralization, oven-dried at 110 ºC till attaining a fixed mass, and lastly preserved in a airtight container for subsequent use (Hussein and Fadhil, 2021). The AC yield was calculated using the following formula (Fadhil and Kareem, 2021):

$$AC\ yield\ (\%) = \frac{Mass\ of\ AC\ produced}{Mass\ of\ mixed\ DSPET\ used} \times 100 \quad (1)$$

Analysis and characterization of AC from mixed DS+PET

The N_2 adsorption-desorption isotherms (77 K) were utilized to examine the sample's surface area and porosity on a BELSORP MINI II, Japan surface area and porosimetry analyzer. The BET (Brunauer-Emmett-Teller) method was implemented to specify the total surface area of the AC in the provided pressure range ($0.005 \leq p/po \leq 0.05$). The surface texture besides the microstructure of microporous AC, were examined using Field Emission scanning electron microscopy (FESEM, Tescan Mira Fesem, Czech Republic). Meanwhile, an elemental analysis of the AC was performed utilizing the energy-dispersive analysis X-ray (EDX) technology. A Malvern panalytical X-ray diffractometer (UK) with a Cu-Kα radiation at λ = 0.15418 nm was employed in specifying the crystal structure of the as-created AC. The most effective surface efficient groups on sorbent surfaces were identified using an FTIR spectrophotometer (JASCO V-630, USA). Samples were diluted with KBr, and the spectra were collected at 400–4000 cm^{-1}. The AC's iodine number (IN) was determined using GB/T 12496.8–2015 (Zhang et al.,2018). The AC surface groups (acid and basic) were quantified by titration with a solution of NaOH or HCl (Boehm, 2002). Lastly, the pHP_{PZC} of the AC surface was specified as well (Yağmur and Kaya, 2021).

Preliminary adsorption studies

The stock solution of DBT (500 mg/L) was first prepared through dissolving the required mass of DBT in a 1L of the solvent (n-hexane). A 250 mL round bottom flasks were implemented batch mode adsorption examinations of DBT for a temperature-controlled stirrer bath. From the stock solution, solutions of multiple concentrations were prepared, and their absorbance were specified to prepare the standardization curve. The solutions' absorbance was measured at the

proper wavelength (λ_{max}= 325 nm) (Hussein and Fadhil, 2021; Moosavi and Karimzadeh, 2015). A constant weight of the AC was mixed with 25 mL of the model, followed by shaking at 35 °C at 150 rpm until reaching equilibrium. Centrifugation was implemented to strip the AC particles from DBT solution for 5 min at 5000 rpm. The residual concentrations of DBT was measured photometrically on a double-beam UV-Vis spectrophotometer (Shimadzu, UV-Visible-160, Japan) at the specified λ_{max}. Trials were completed in triplicate, and their outcomes were presented as the mean SD. The adsorption process was expanded to examine the effect of pollutant starting concentration (25–200 mg/L), mass of AC (0.05–0.50 g), operational temperature (15–45 °C), and the adsorption duration (5–120 min) on the ADS% of DBT from the model. Eq.(2) was employed in specifying the adsorption capacity of the AC to DBT, while Eq.(3) was followed on determining the ADS%.

$$q_e = \frac{(C_o - C_e)\,V}{W} \tag{2}$$

$$ADS\ (\%) = \frac{(C_o - C_e)}{C_o} \times 100 \tag{3}$$

where: C_o and C_e denote respectively the initial and equilibrium concentrations of the DBT (mg/L), whereas V, and W, are volume of pollutant used in the adsorption experiment and mass of AC implemented.

Reusability experiments

Regenerating the AC specimens consumed upon stripping DBT from the model was accomplished through placing the collected specimens into a Soxhlet extractor so as to eliminate the adsorbed DBT employing n-hexane as a solvent, followed by drying the regenerated AC at 105 °C for 2 h. After drying, the AC was finally reactivated at 500 °C for 30 min to be reemployed later in the ADS process for several cycles (Mohammed-Taib and Fadhil, 2023).

RESULTS AND DISCUSSION

Effect of preparation conditions on AC yield and porosity

The optimized protocol was followed to synthesize AC samples from mixed DSPET using $ZnCl_2$ as an activator. In this regard, the effect of the IR of $ZnCl_2$, temperature of activation, and period of activation, on the yield and IN of the AC samples, were inspected. Fig. 1a depicts the IR influence of $ZnCl_2$ on the AC yield. This figure showed that with the increase of the IR of the activator, the AC output decreased. Such findings belong to the fact that increasing the activator IR will remove further volatile substances, including H_2O, CH_4, CO, CO_2, tar, and aldehydes from the precursor structure may be as an outcome of the degradation, dehydration, and condensation reactions of the mix (Nayak and Pal, 2020). Such reactions may result in facilitating the condensation reactions of aromatic between neighboring molecules, leading to further gasification of the precursor structure besides a decline in AC yield (Nayak and Pal.,2020, Olorundare et al., 2014). Synthesis of AC from biochar from mixed date seeds and olive stones (Fadhil and Kareem, 2021), liquefied wood (Liu et al., 2016), and peat (Varila et al., 2017) by the $ZnCl_2$-activation disclosed similar findings. Microporous structure of the AC can be expressed by the IN. As per Fig. 1a, a positive increase in the IN of the AC samples was observed with rising the IR of $ZnCl_2$ from 0.5:1 to 2:1. This outcome can be ascribed to the additional releasing of the volatile substances (H_2O, CH_4, CO, CO_2, aldehydes, tar, etc.) from the carbon framework of the raw feed, resulting in the creation of novel micro-porous carbon (Xia et al., 2014). The IN decreased when the IR surpassed 2.0 might be due to the probability of pore obstruction caused by devolatilizing of tarry materials besides other volatiles generated upon the carbonization reaction (Mohammed-Taib and Fadhil, 2023; Hussein and Fadhil, 2021). Comparable outcomes have also declared by several authors during the creation of AC samples from different precursors using the $ZnCl_2$-activation route (Mohammed-Taib and Fadhil, 2023; Fadhil and Kareem, 2021; Hussein and Fadhil, 2021).

As presented in Fig. 1b, a decrease in the AC yield was noticed with ascending temperature of activation from 400 °C to 800 °C, because of several reactions may occur to the impregnated samples, including breakdown, devolatilization, and dehydration (Varila et al., 2017). Such results were in line with those announced by several investigators upon the creation of different AC samples from various precursors by the $ZnCl_2$-activation method (Hussein and Fadhil, 2021; Liu et al., 2014). The increase in temperature during activation led to a more efficient removal of volatile

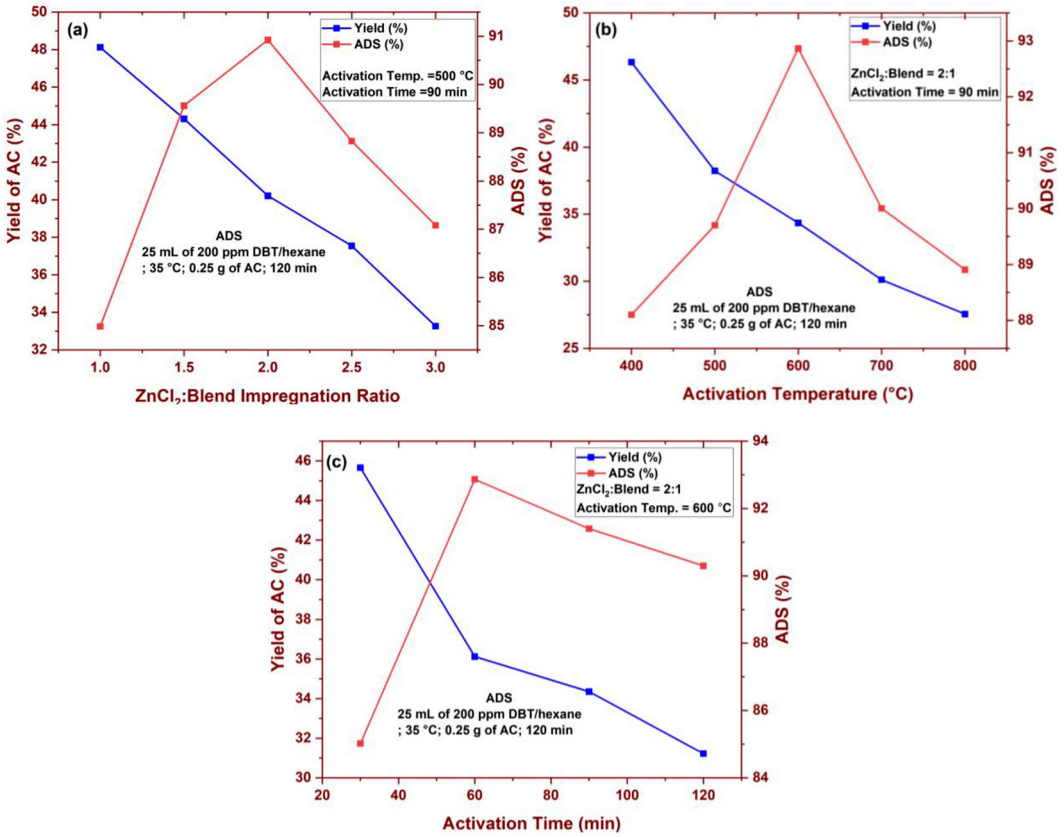

Figure 1. Effect of the preparation conditions of AC on its yield and its ADS performance

substances, and thus caused an increase in the IN of the AC because of the formation of a new microporous structure (Liu et al., 2014). The maximum was observed with the AC sample activated in 600 °C, while samples activated at temperatures above 600 °C exhibited lower IN due to the disintegration of micropores walls, as well as the conversion of micropores into bigger pores (meso and macropores) (Danmaliki and Saleh, 2016; Liu et al., 2014). Our findings were in agreement with those established by other authors upon creating various samples of the AC from multiple raw materials via the $ZnCl_2$-activation (Hussein and Fadhil, 2021; Danmaliki and Saleh, 2016; Liu et al., 2014)

Several durations (30–120 minutes) were examined to realize its impression on both the AC yield and IN. Fig. 1c exhibited that time possessed an undesirable effect on the AC yield. The longer activation period increased dryness of the feed, and lessened the yield (Mohammed-Taib and Fadhil, 2023; Liu et al., 2016). As a result of the additional dehydration of the material, prolonging the period of activation led to the formation of additional micropores in the AC frame, which increased the IN (Mohammed-Taib and Fadhil, 2023; Hussein and Fadhil, 2021). Beyond the typical period of activation, the IN dropped, because micro-pores expanded or altered into bigger pores (Demiral et al., 2016). The attained result was consistent with those reported by other authors (Mohammed-Taib and Fadhil, 2023; Ganiyu and Lateef, 2021; Hussein and Fadhil, 2021).

The AC characterization

The ideal sample of the AC created at the optimum experimental conditions of 2:1 $ZnCl_2$: feed, 600 °C, and 60 min, was thoroughly identified diagnosed by numerous techniques to examine its texture, morphological, and amorphous features. Fig. 2a displays the N_2 adsorption-desorption isotherms in addition to the pore size distributions for the AC. The isothermal profile of the AC displayed in Fig. 2a can be categorized as Type IV along with H_4 hysteresis as an outcome of the filling of micropores at a low relative pressure (P/P_o). This conclusion was made based on the mismatch between the both isotherms. Also, at a P/P_o value above 0.4, the AC exhibited a small hysteresis loop, indicating the presence of wider microporosity and mesoporosity. When the

ratio of P/P_o exceeds 1.0, the empty spaces between the AC particles will be occupied by molecules of N_2, and thus raised the adsorbed volume (Neme et al.,2022). In accordance to the results shown in Table 1, the as-created AC exhibited a specific surface area (SA_{BET}) of 672.22 m^2/g. By comparison, the synthesized AC exhibited a BJH surface area of 297.30 m^2/g and an average pore width of 3.16 nm (Fig. 2b). The ratio of mesoporosity in the AC as per the BJH surface area was 55.77%. Thus, it can be said that the structure of the as-prepared AC contains both micropores and mesopores. The AC samples developed from various feedstocks and prepared via the $ZnCl_2$-activation route showed similar ADS activity for DBT from model fuel. Wild mustard stems-derived mesoporous AC had a SA_{BET} of 1280.0 m^2/g and an average pore size of 3.69 nm. This mesoporous AC exhibited an excellent ADS% of DBT from model fuel (96.02%)(Mohammed-Taib and Fadhil., 2023). The biochar derived by thermal pyrolysis of mixed DS and olive stones, was activated with $ZnCl_2$ and the produced AC had a SA_{BET} of 936.48 m^2/g with an average pore size of 2.53 nm. This AC also exhibited an effective efficiency toward the ADS of DBT from model oil (Fadhil and Kareem, 2021). In another study, AC synthesized by the $ZnCl_2$-activation of mixed DS and olive stones possessed a SA_{BET} of 1389.90 m^2/g with an average pore size of 1.21 nm, and showed an energetic activity in the ADS of DBT from fuel (Hussein and Fadhil, 2021). As such, it is possible to say that the ADS of DBT from transportation fuel requires an AC with a well-developed porous structure besides high SA_{BET}. Fig. 2c shows the FESEM image of the AC synthesized by the $ZnCl_2$-activation of mixed DSPET. The AC exhibited a rough and irregular surface. Also, some grains besides round-shaped cavities could be seen at its surface. Irrespective of the variation in pore size, the $ZnCl_2$ -activation of the mix at the given IR led to create pores with a different shapes and sizes. Holes and interior surface area are essential prerequisites for AC to be considered a highly effective adsorbent, especially for adsorption in the liquid phase. Therefore, it is possible to say that the occurrence of such cavities will make the penetration of the pollutant molecules inside them easier, contributing to a better adsorption efficiency. The EDX profile of the as-prepared AC (Fig. 2c) revealed that the AC was chiefly composed of C and O. The high C% in the AC revealed that the activator had completely carbonized the original feed through removing its volatile materials and forming carbon with a highly porous structure. These results are compatible with the SA_{BET} and FESEM image of the AC. Also, elements belong to the activator (Zn and Cl) could not be detected in the EDX map of the AC, assuring that it was entirely consumed upon the carbonization of the parent feed into AC. Besides, the occurrence of O in the composition of AC demonstrates that its surface will contain numerous oxygenated functional groups, which help remove DBT from liquid fuel.

The FTIR measurements of the AC developed from mixed DSPET (Fig. 2d) exhibited the occurrence of many functional groups on its surface, like the that broad at 3423 cm^{-1}, which represents the stretching vibration band of O-H group in various oxygenated compounds, including H_2O, Ph-O-H, RC=O–O–H, and R-O-H (Xiong et al.,2021). The absorption peak between 2922 cm^{-1} and 2852 cm^{-1} ascribe to the (C–H) stretching vibrations in CH_3 and CH_2 groups (Wang et al., 2014). The stretching mode of the C=O group in esters, acids or lactones is that peak noticed at 741 cm^{-1} (Wang et al., 2014; Guo et al., 2020). The C=C group stretching vibration in an aromatic skeleton can be expressed by the peak seen at 1854 cm^{-1} (Wang et al., 2014). The C-O group stretching vibration can be assigned by the peak noticed at 1392 cm^{-1} (Guo et al., 2020), while the stretching mode of vibration of the C-O-C bond could be presented by the bands seen between 1008 cm^{-1} and 1249 cm^{-1} (Wang et al., 2014).

Finally, the distinguishing peak detected at 620 cm^{-1} may ascribe to the bending mode of vibration of the C–H group (Guo et al., 2020). The adsorptive ability of the AC on eliminating multiple pollutants via various axillary processes will be enhanced by the presence of multiple effective groups on the AC surface. Fig. 2e, which depicts the XRD pattern of the AC showed the existence two broad peaks at $2\theta = 22.50°$ and $2\theta = 43.40$, which are respectively assigned to (002) and (100) reflections, and corroborate the amorphous and graphitic nature of the AC adsorbent. Titration was used to determine the total acid and basic groups on the AC surface, which were determined to be 0.3160 and 0.0511 (mmol/g), respectively. Such results indicate that the surface of the AC originating from mixed DSPET, has an acidic character. Our finding was comparable to those announced for AC samples prepared through the $ZnCl_2$-activation route (Hussein and Fadhil,

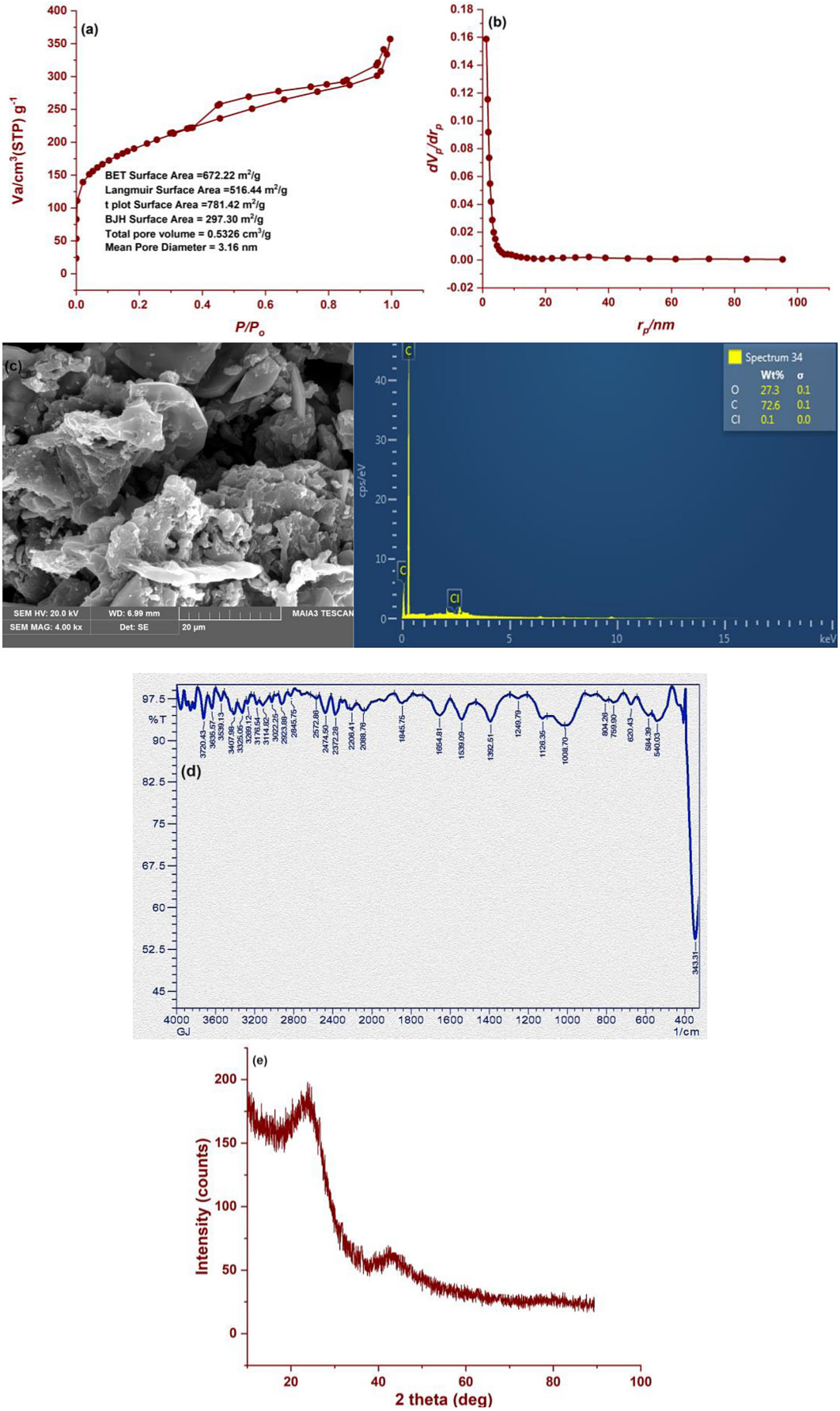

Figure 2. The N_2 adsorption-desorption isotherms, pore size distribution, FESEM-EDX images, FTIR spectrum, and XRD pattern of the AC

2021). The pH_{PZC} (point of zero charge) is a crucial element because of its significance in the adsorption process of different contaminants by diverse adsorbents. It demonstrates the pH value at which the total charge on the surface of a given adsorbent is zero. The pH of the as-obtained AC was 5.80, which aligns with the results of the surface groups, confirming that the surface of the AC is acidic.

The ADS experiments

An investigation was conducted to examine the impact of the working variables on DBT stripping from the model utilizing the AC developed from the said mix of wastes. The initial concentration influence of DBT on the adsorptive capacity of the AC (q_e, mg/g) besides the ADS% from the fuel is presented in Fig. 3a. The latter implied that increasing the DBT initial concentration from 25 mg/L to 200 mg/L raised the q_e value from 2.20 mg/g to 16.0 mg/g as an outcome of increasing the number of DBT species per mass unit of AC, casing improved interactions between the DBT molecules and the AC particles (Hussein and Fadhil, 2021). Furthermore, raising the sorbate starting concentration will provide the required motivation to minimize resistance between the DBT liquid phase and the AC solid phase (Mohammed-Taib and Fadhil, 2023). As seen in Fig. 3a, the ADS% of DBT decreased as the DBT initial concentration increased. This behavior can be clarified by the fact that the number of energetic positions accessible to DBT adsorption remains unchanged while the number of DBT species grows with increasing the DBT concentration. Consequently, the ADS% will decrease as the active sites are gradually depleted (Yaseen et al., 2021). Multiple dosages (0.05–0.50 g) of the AC were tried to explore the influence of this parameter as a consequence of its potential effect on DBT removal. The experiments were conducted applying the conditions described in Fig. 3b legend. The attained outcomes suggested that rising the AC dose from 0.05 g to 0.35 g resulted in an increase in ADS% from 55.42% to 92.21%. The elevated ADS% of DBT with increasing the AC dosage may be explained by the fact that a greater number of AC particles are present with using

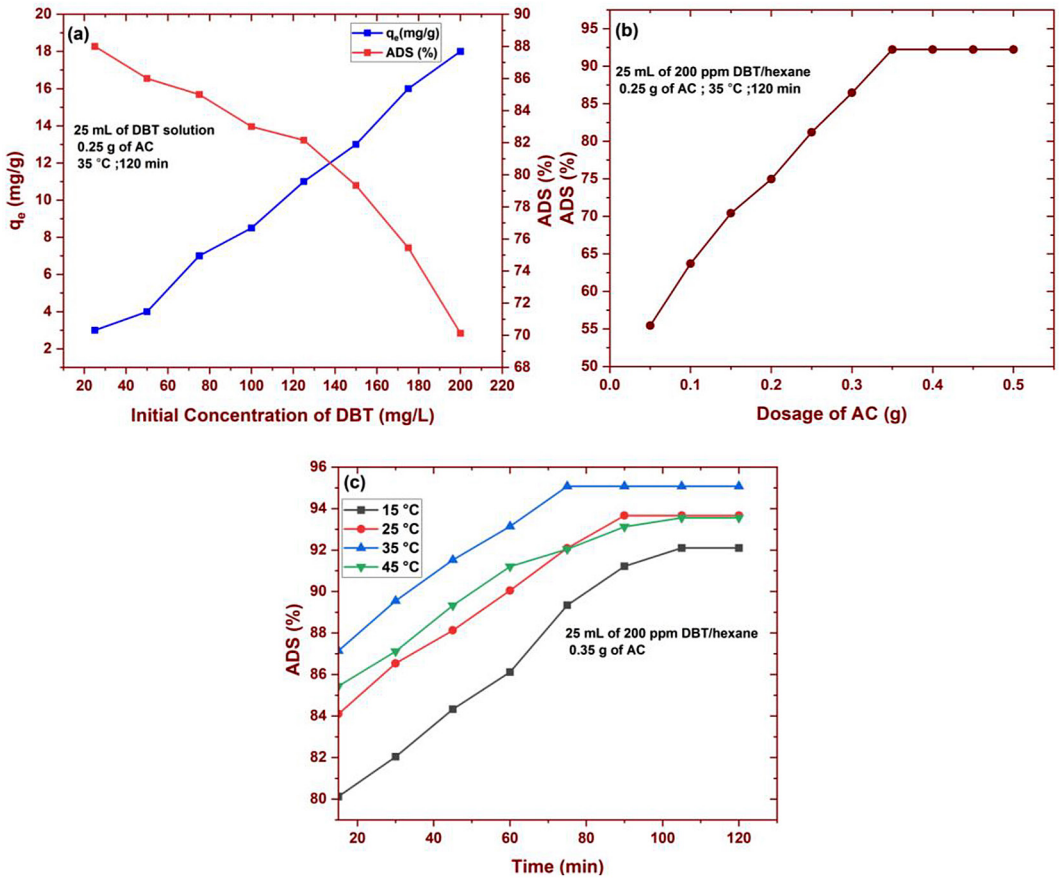

Figure 3. Effect of the adsorption parameters on the ADS % of DBT by the AC

further dosages of AC, leading to a higher SA and more active sites accessible to adsorb the DBT species from the fuel (Yaseen et al., 2021). Trying dosages above 0.35 g exhibited no influences on the ADS of DBT as the system was attained equilibrium. Other researchers have announced comparable consequences (Mohammed-Taib and Fadhil, 2023; Fadhil and Kareem, 2021, Hussein and Fadhil, 2021). Four different temperatures (15 °C,25 °C,35 °C, and 45 °C) were tried in examining the temperature's effect on the ADS% of DBT from the fuel. The trials were completed under the parameters specified in the legend of Fig. 3c. The outcomes offered in Fig. 3c indicated to an increase in the ADS% of DBT with the rise of temperature because of the increase in entropy of the system, which promotes collisions between the species of DBT with the AC particles (Ma et al., 2017). Maximum ADS% was noticed at 35 °C, while higher temperature caused a diminish in the ADS% of DBT. Furthermore, when the system temperature rises, the solution viscosity decreases, and consequently improves collisions between the two phases (Yaseen et al., 2021; Hussein and Fadhil., 2021). Besides, the ADS% enhancement with expanding temperature clarifies that DBT adsorption by the said AC is endothermic. Temperature beyond 35 °C dropped the ADS% of DBT may be due to higher temperature may weaken the attraction forces between the activate sites on the AC surface and the DBT species, leading to a lower ADS% (Ma et al., 2017).

Time intervals between 5 and 120 min were examined to assess the contact time influence on the ADS% of DBT form the fuel, with applying the optimal working conditions found earlier, as offered in Fig. 3c. Longer contact time between the two phases resulted in a greater removal DBT by the AC. Also, high uptake of the DBT was observed after 60 minutes of the process, suggesting that ADS process is spontaneous. In the initial steps of the ADS process, the latter was rapid as an outcome of the larger surface area of the AC surface, which is beneficial in receiving more species of the DBT species. After a certain duration, equilibrium was attained due to the occupation of most of the vigorous positions of the AC surface by the DBT species. Thus, adsorbing more DBT species will be rendered. This could result in a repulsive force between the adsorbate on the surface of AC and adsorbate in the fuel phase (Mohammed-Taib and Fadhil, 2023; Shah et al., 2015).

Isothermal studies of the ADS process

Analyzing the adsorption isotherms of the adsorbate adsorption by an adsorbent surface assist in identifying the adsorption mechanism(Fadhil and Kareem, 2021). As a result, the Langmuir (Fig. 4), Freundlich (Fig. 4), and Temkin (Fig. 4) isotherms, were applied to explore the DBT sorption on the AC from the said mix of waste. The linear form of this Langmuir isotherm is given in Eq.(4):

$$\frac{C_e}{q_e} = \frac{1}{q_m K_L} + \frac{C_e}{q_m} \tag{4}$$

where: q_m – represents the amount of DBT needed to form a complete monolayer coverage (mg/g) on the AC surface, while K_L is the Langmuir constant. Theoretically, monolayer adsorption onto a solid surface is suggested by the Langmuir model. The lessening of interactions between pollutant species is also indicative of the efficiency of the active sites in adsorption (Yaseen et al., 2021).

The Langmuir constants, namely q_m and K_L were respectively resulted from the slope and intercept of the plot, while the dimensionless separation factor (R_L) was determined using the following formula:

$$R_L = \frac{1}{1 + C_0 K_L} \tag{5}$$

The adsorbate's affinity for the adsorbent surface can be expressed by this factor. This component also suggests several instances of the adsorption process, e.g., the adsorption will be preferable when $0 < R_L < 1$. If $R_L > 1$, the adsorption will be unprofitable.

According to the Freundlich model, multilayer adsorption on the solid surface occurs. It also posits that the solid surface is heterogeneous, with different-affinity active spots appearing on the material surface (Xia et al., 2014).The linear form of this isotherm is given in Eq. (6):

$$ln\, q_e = ln\, K_F + \frac{1}{n} ln\, C_e \tag{6}$$

where: n and K_F are the Freundlich constants, which respectively signify the adsorption intensity and capability. The Freundlich constants viz. n and K_F, can be deduced from the slope and the intercept of the linear plot. The value of n, which indicates the adsorption favorability. It suggests

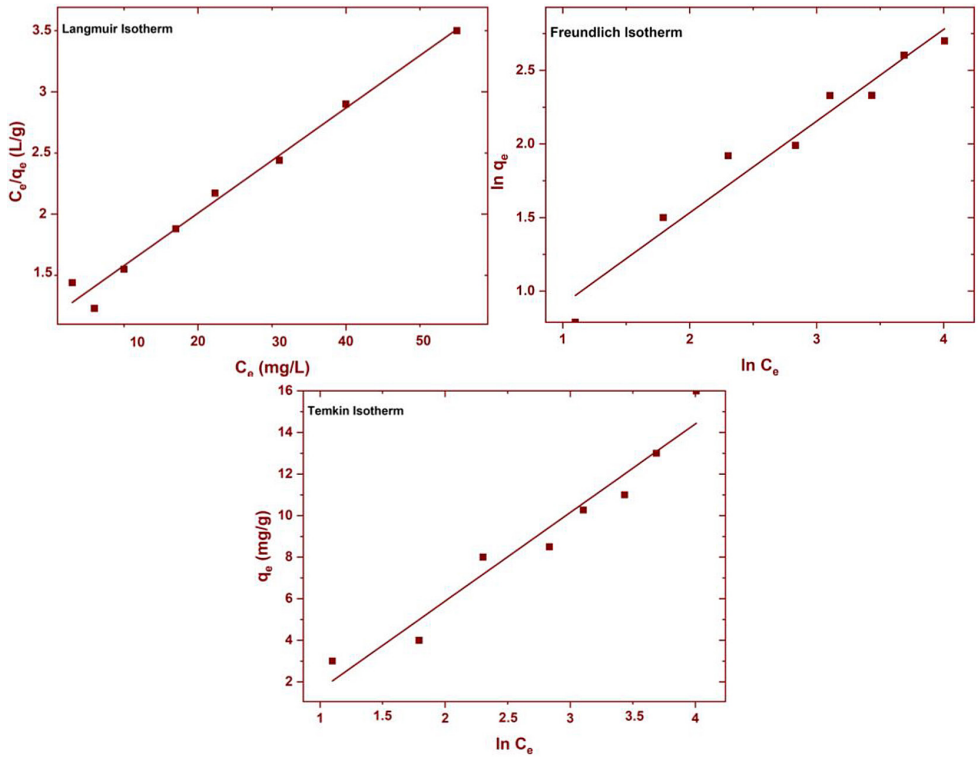

Figure 4. Adsorption isotherms of DBT by the AC

that when n >1.0, the adsorption will be profitable onto a solid surface.

The Temkin model, which asserts that the heat of adsorption declines as the surface of the adsorbent is covered adsorbate species, may reflect the interaction between the adsorbent and adsorbate irrespective of the extremely high and low concentrations (Yaseen et al., 2021). The linear form of this isotherm is given in Eq. (7):

$$q_e = \frac{RT}{b} ln\, KT + \frac{RT}{b} ln\, C_e \qquad (7)$$

where: K_T, and b indicate respectively the equilibrium binding constant (L/g) and the heat of adsorption (J/mol). The slope and intercept of the Temkin linear plot will yield B and K_T values.

According to the results offered in Table 1, the Langmuir model had higher R^2 values than the Freundlich and Temkin models. Furthermore, the q_m value for the Langmuir model was higher than those found for K_F and B, indicating that the Langmuir model can better explain DBT adsorption by the derived AC than the Freundlich and Temkin models. The results above confirmed that adsorbing DBT by surface of the AC happens in a monolayer. Furthermore, because adsorption occurs onto active sites with the same energy, interactions between the DBT molecules are hindered (Deb et al., 2021).

Kinetics and thermodynamic studies of the ADS process

Aside from the equilibrium time, the efficiency of the adsorption process can be further explained by understanding the adsorption kinetics besides describing the rate of adsorption onto the adsorbent surface (Ibrahim et al., 2022). Consequently, three well-known models viz. the pseudo-1st-order model, pseudo-2nd-order model, and the intra-particle diffusion model, were applied to analyze DBT adsorption data by the produced AC, in order to figure out the stages governing the adsorption of DBT on the AC. The DBT adsorption on the aforementioned AC was performed at three different temperatures (288 K, 298 K, and 308 K). The data collected were examined using the linear forms of those models. The correlation coefficient (R^2), q_e (mg/g), k_1 (min^{-1}), and k^2 values for the pseudo-1st-order and pseudo-2nd-order models were calculated from the plot slope and intercept, respectively. According to the results in Table 2, the R^2 value for the pseudo-2nd-order model was above that

Table 1. Values of the adsorption isotherms constants for DBT adsorption

Langmuir constants				Freundlich constants			Temkin constants		
R^2	q_m (mg/g)	K_L	R_L	R^2	n (mg/g)	K_F	R^2	B	A
0.9846	23.80	0.0367	0.1199	0.9590	0.5727	0.4949	0.8572	0.9963	0.1175

belongs to the pseudo-1st-order model, showing that the former model can accurately represents the DBT adsorption by the so-prepared AC. Furthermore, the q_e value for the pseudo-2nd-order model was closer to that derived from the adsorption isotherm. Weber's intra-particle diffusion model was also tried to analyze the DBT experimental adsorption data. This model can predict processes and rate-controlling phases that influence DBT adsorption kinetics. Because none of the regression plots pass through the origin, it is clear from Fig. 4, which depicts The intra-particle diffusion model, that this model cannot be used solely to describe the rate-limiting step of DBT adsorption by the derived AC (Yaseen et al., 2021; Fadhil and Kareem, 2021).

The thermodynamic parameters ΔH, ΔS, and ΔG, were have also calculated based on the adsorption outcomes of DBT on the AC. In addition to spontaneity, these functions may offer insights into the adsorption process, such as exothermicity or endothermicity, possible increase or decrease in disorder at the solid/liquid interface (Hussein and Fadhil, 2021). These functions can also be exploited to explain the adsorption mechanism. These functions for DBT adsorption by the AC were calculated at three different temperatures, 288 K, 298 K, and 308 K. The following equations were employed in calculating ΔH_o, ΔS_o, and ΔG_o of DBT adsorption on the AC:

$$ln(K_c) = \frac{\Delta S_o}{R} - \frac{\Delta H_o}{RT} \quad (8)$$

$$\left(\frac{q_e}{C_e}\right) = K_c \quad (9)$$

$$\Delta G_o = -RT\, ln\, K \quad (10)$$

where: K_c indicates the equilibrium constant. Plotting ln K_c vs 1/T yields a straight line. The slope of this linear plot gives ΔH°, while ΔS° can be deduced from the intercept following the van't Hoff equation.

Table 3 displays the ΔH°, ΔS°, and ΔG° data for DBT adsorption on the AC, revealing that the adsorption was endothermic. This result was reached based on the ΔH° value (9.51 kJ/mole), demonstrating that the DBT adsorption by this AC is temperature-dependent and endothermic. This outcome was anticipated due to the increased adsorption of DBT by the AC when the temperature rose from 288 K to 308 K. Furthermore, the DBT adsorption by the derived AC was spontaneous due to the -ve values of ΔG° at different temperatures. As per literature, when the values of ΔG° are in the range of (-20 to 0.0 kJ/mol), the adsorption is physical, but values in the range of (-400 to -80 kJ/mol) suggest chemisorption(Dutta et al.,2022). As the ΔG° values for the DBT adsorption by the AC ranged from -2.56 to -3.46 kJ/mol, it can be

Table 2. The kinetics models values for the adsorption of DBT

T = 288 K								
Psedue-1st-order			Psedue-2nd-order			Intra-particle diffusion		
R^2	q_e (mg/g)	k_1	R^2	q_e (mg/g)	k_2	R^2	C	K_{id}
0.9698	2.12	0.0009	0.9999	13.51	0.0481	0.5267	6.06	0.8241
T = 298 K								
Psedue-1st-order			Psedue-2nd-order			Intra-particle diffusion		
R^2	q_e (mg/g)	k_1	R^2	q_e (mg/g)	k_2	R^2	C	K_{id}
0.9537	2.20	0.0010	0.9999	13.88	0.0405	0.5236	6.23	0.8307
T = 308 K								
Psedue-1st -order			Psedue-2nd -order			Intra-particle diffusion		
R^2	q_e (mg/g)	k_1	R^2	q_e (mg/g)	k_2	R^2	C	K_{id}
0.9000	2.33	0.0009	0.9999	14.47	0.0505	0.5151	6.37	0.8352

Table 3. Thermodynamic functions values for DBT adsorption by the AC

Temperature (K)	$\Delta G°$ (kJ. mol^{-1})	$\Delta S°$ (kJ.mol^{-1}. K^{-1})	$\Delta H°$(kJ. mol^{-1})
288	-0.0474	0.0650	18.80
298	-0.0552	-	-
308	-1.357	-	-

said that DBT adsorption by the AC is physical, which accomplished via the electrostatic attraction and H-bonding (Dutta et al., 2022).

Comparison of the ADS performance

Table 4 compares the ADS% and q_e (mg/g) for DBT by AC generated from the aforementioned blend of solid wastes with those achieved by other adsorbents in the literature. The AC prepared here had an ADS% and q_e value comparable to other adsorbents announced in the literature, and in some cases better. The differences in the ADS% and q_e value of DBT adsorption by various adsorbents can be attributed to a variety of parameters, including the adsorbent's SA_{BET}, pore width, total pore volume, and the number of acidic or basic groups on its surface. These factors along with the volume of the DBT solution used besides the type of mechanism engaged in the adsorption process

Table 4. Comparison between the ADS % of the AC and other adsorbents

Adsorbent	Initial Conc. of S-compound	Dosage (g)	Temperature (°C)	Time (min)	ADS (%)	q_e (mg/g)	Ref.
AC from corn cobs	200 mg/L DBT	0.015	30	120	-	19.10	(Yaseen et al., 2021)
AC from wild mustard stems	200 mg/L DBT	0.40	30	30	96.02	71.42	(Mohammed-Taib and Fadhil, 2023)
AC from biochar from mixed biowastes	200 mg/L DBT	0.30	50	90	90.01	41.66	(Fadhil and Kareem, 2021)
AC from mixed biowastes	200 mg/L DBT	0.30	40	60	92.86	45.24	(Hussein and Fadhil, 2021)
Leaf of *Punica granatum*	1000 mg/L DBT	1.0	30	60	70.55	55.55	(Sadare and Daramola, 2019)
AC from palm shell	10 mg/L DBT	0.10	25	35	91.50	2.75	(Anisuzzaman, 2017)
AC from mixed DSPET	200 mg/L DBT	0.35	35	80	95.07	23.80	This study

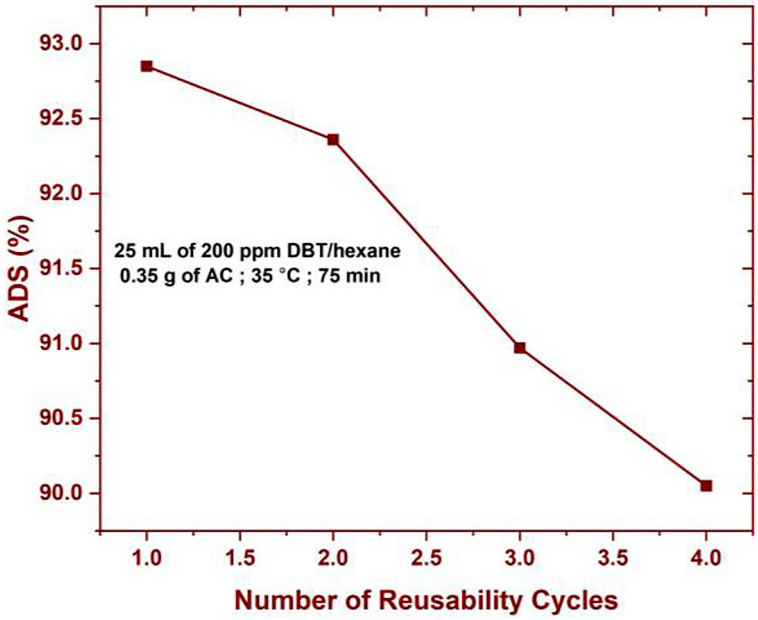

Figure 5. Reusability cycles of the AC

all have an impact on the ADS% and q_e value of DBT by any specific adsorbent.

Regeneration and reusability studies

The exhausted specimens of the AC were gathered so as to assess the possibility of regenerating and reusing of the AC due to the importance of this issue from an economical point of view. The exhausted AC specimen was placed into a Soxhlet extractor to strip the adsorbed DBT from the AC employing n-hexane as the solvent. After eliminating the DBT from the AC, the latter was implemented in the ADS of DBT under the previously reported typical conditions after drying at 105 °C for 2h (Hussein and Fadhil, 2021). In each reusability cycle, this process was repeated. The results offered in Fig. 5 revealed that extending the reusability cycles resulted in a modest decrease in DBT R%. The ADS% of DBT amounted to 97.22% in the 1st cycle compared to 89.21% in the 5th, indicating that the AC surface still has accessible locations suited to eliminate DBT molecules. As a result, the obtained results suggested that the AC developed from the said blend of solid wastes is a good adsorbent for purifying transportation fuels from S-compounds.

CONCLUSIONS

The utilization of an equal mixture of DS and PET wastes led to synthesize an AC with a reasonable surface area and mesoporous structure through the $ZnCl_2$-activation process. The so-prepared AC had a BET surface area of 672.22 m^2/g and a mean pore width of 3.16 nm. Adsorbing DBT from a model oil was made by employing the as-created AC showed the highest ADS% (95.07 %) using 0.30 g of the AC at 35 °C for 80 min with a 23.80 mg/g adsorptive capacity. The AC produced from the suggested precursor best manifested that the DBT adsorption followed the Langmuir adsorption isotherm and pseudo-2nd-order kinetics model. The effectiveness of the produced AC was demonstrated by the regenerated AC activity, which showed an outstanding adsorptive performance for DBT up to four cycles of reuse.

Acknowledgment

The authors are very thankful to Mosul University, College of Science, Chemistry Department to make this research work successful.

REFERENCE

1. Ahmed, M.J., & Theydan, S.K., 2015. Adsorptive removal of p-nitrophenol on microporous activated carbon by FeCl3 activation: equilibrium and kinetics studies. Desalination and Water Treatment, 55(2), 522-531.
2. Alhamed, Y.A., Bamufleh, H.S., 2009. Sulfur removal from model diesel fuel using granular activated carbon from dates' stones activated by ZnCl2. Fuel, 88(1), 87-94.
3. Ali, F. D. 2018. Adsorptive desulfurization of liquid fuels using Na-bentonite adsorbents. Al-Nahrain Journal for Engineering Sciences, 21(2), 248-252
4. An, H.J., Bhadra, B.N., Khan, N.A., & Jhung, S.H., 2018. Adsorptive removal of wide range of pharmaceutical and personal care products from water by using metal azolate framework-6-derived porous carbon. Chemical Engineering Journal, 343, 447-454.
5. Anisuzzaman, S.M., 2017. Adsorptive desulfurization of model fuel by activated oil palm shell. Indian Journal of Chemical Technology (IJCT), 24(2), 206-212.
6. Arslanoğlu, H., Orhan, R., & Turan, M.D., 2020. Application of response surface methodology for the optimization of copper removal from aqueous solution by activated carbon prepared using waste polyurethane. Analytical Letters, 53(9), 1343-1365.
7. Bamufleh, H.S., 2009. Single and binary sulfur removal components from model diesel fuel using granular activated carbon from dates' stones activated by ZnCl2. Applied Catalysis A: General, 365(2), 153-158.
8. Boehm, H.P., 2002. Surface oxides on carbon and their analysis: a critical assessment. Carbon, 40(2), 145-149.
9. Danmaliki, G.I., & Saleh, T A., 2016. Influence of conversion parameters of waste tires to activated carbon on adsorption of dibenzothiophene from model fuels. Journal of Cleaner Production, 117, 50-55.
10. de la Cruz, A.B., Boahene, P., Vedachalam, S., Dalai, A.K., & Adjaye, J., 2020. Adsorptive desulfurization through charge-transfer complex using mesoporous adsorbents. Fuel, 269, 117379.
11. Deb, A., Debnath, A., & Saha, B., 2021. Sono-assisted enhanced adsorption of eriochrome Black-T dye onto a novel polymeric nanocomposite: kinetic, isotherm, and response surface methodology optimization. Journal of Dispersion Science and Technology, 42(11), 1579-1592.
12. Dehghan, R., & Anbia, M., 2017. Zeolites for adsorptive desulfurization from fuels: A review. Fuel Processing Technology, 167, 99-116.
13. Demiral, I., Aydın Şamdan, C., & Demiral, H., 2016. Production and characterization of activated carbons from pumpkin seed shell by chemical activation with ZnCl2. Desalination and Water Treatment,

57(6), 2446-2454.

14. Deng, L., Guo, W., Ngo, H.H., Zhang, X., Wei, D., Wei, Q., & Deng, S. (2023). Novel catalysts in catalytic upcycling of common polymer wastes. Chemical Engineering Journal, 144350.
15. Diaz, E., Sanchis, I., Coronella, C.J., & Mohedano, A.F., 2022. Activated carbons from hydrothermal carbonization and chemical activation of olive stones: application in sulfamethoxazole adsorption. Resources, 11(5), 43.
16. Dutta, S.K., Amin, M.K., Ahmed, J., Elias, M., & Mahiuddin, M., 2022. Removal of toxic methyl orange by a cost-free and eco-friendly adsorbent: Mechanism, phytotoxicity, thermodynamics, and kinetics. South African Journal of Chemical Engineering, 40, 195-208.
17. Fadhil, A.B., & Kareem, B.A., 2021. Co-pyrolysis of mixed date pits and olive stones: Identification of bio-oil and the production of activated carbon from bio-char. Journal of Analytical and Applied Pyrolysis, 158, 105249.
18. Ganiyu, S.A., & Lateef, S.A., 2021. Review of adsorptive desulfurization process: Overview of the non-carbonaceous materials, mechanism and synthesis strategies. Fuel, 294, 120273.
19. Guo, Y., Tan, C., Sun, J., Li, W., Zhang, J., & Zhao, C., 2020. Porous activated carbons derived from waste sugarcane
20. Hussein, A.A., & Fadhil, A.B., 2021. Kinetics and isothermal evaluations of adsorptive desulfurization of dibenzothiophene over mixed bio-wastes derived activated carbon. Energy Sources, Part A: Recovery, Utilization, and Environmental Effects, 1-20.
21. Hussain, S., Kamran, M., Khan, S.A., Shaheen, K., Shah, Z., Suo, H.,... & Ghani, U., 2021. Adsorption, kinetics and thermodynamics studies of methyl orange dye sequestration through chitosan composites films. International Journal of Biological Macromolecules, 168, 383-394.
22. Hou, L.P., Zhao, R.X., Li, X.P., & Gao, X.H., 2018. Preparation of MoO2/g-C3N4 composites with a high surface area and its application in deep desulfurization from model oil. Applied Surface Science, 434, 1200-1209.
23. Keppetipola, N.M., Dissanayake, M., Dissanayake, P., Karunarathne, B., Dourges, M.A., Talaga, D., & Cojocaru, L., 2021. Graphite-type activated carbon from coconut shell: a natural source for eco-friendly non-volatile storage devices. RSC advances, 11(5), 2854-2865.
24. Liu, S.L., Wang, Y.N., & Lu, K.T., 2014. Preparation and pore characterization of activated carbon from Ma bamboo (Dendrocalamus latiflorus) by H3PO4 chemical activation. Journal of Porous Materials, 21, 459-466.
25. Liu, Z., Huang, Y., & Zhao, G., 2016. Preparation and characterization of activated carbon fibers from liquefied wood by ZnCl2 activation. BioResources, 11(2), 3178-3190
26. Ibrahim, M.A., Shaban, M.A.A., Hasan, Y.R., Hussein, H.A., Abed, K.M., Mohammed, S J.,... & Hasan, H.A. 2022. Simultaneous Adsorption of Ternary Antibiotics (Levofloxacin, Meropenem, and Tetracycline) by SunFlower Husk Coated with Copper Oxide Nanoparticles. Journal of Ecological Engineering, 23(6).
27. Ma, C., Chen, X., Long, D., Wang, J., Qiao, W., & Ling, L., 2017. High-surface-area and high-nitrogen-content carbon microspheres prepared by a pre-oxidation and mild KOH activation for superior supercapacitor. Carbon, 118, 699-708.
28. Moosavi, E.S., & Karimzadeh, R.,2015. Adsorption of thiophenic compounds by OFG-tailored fiber and activated carbons. Separation Science and Technology, 50(13), 1940-1951.
29. Mohammed-Taib, B.M., & Fadhil, A.B. 2023. Dibenzothiophene capture from model fuel by wild mustard stems derived activated carbon: kinetics and isothermal evaluations. International Journal of Environmental Analytical Chemistry, 103(16), 4654-4676.
30. Moreira, A.M., Brandão, H.L., Hackbarth, F.V., Maass, D., de Souza, A.U., & de Souza, S.G.U. 2017. Adsorptive desulfurization of heavy naphthenic oil: equilibrium and kinetic studies. Chemical Engineering Science, 172, 23-31.
31. Nayak, A.K., Pal, A., 2020. Statistical modeling and performance evaluation of biosorptive removal of Nile blue A by lignocellulosic agricultural waste under the application of high-strength dye concentrations. Journal of Environmental Chemical Engineering, 8(2), 103677.
32. Neme, I., Gonfa, G., & Masi, C., 2022. Preparation and characterization of activated carbon from castor seed hull by chemical activation with H3PO4. Results in Materials, 15, 100304.
33. Olorundare, O.F., Msagati, T.A.M., Krause, R.W.M., Okonkwo, J.O., & Mamba, B.B., 2014. Activated carbon from lignocellulosic waste residues: effect of activating agent on porosity characteristics and use as adsorbents for organic species. Water, Air, & Soil Pollution, 225, 1-14.
34. Prakash, M.O., Raghavendra, G., Ojha, S., & Panchal, M., 2021. Characterization of porous activated carbon prepared from arhar stalks by single step chemical activation method. Materials Today: Proceedings, 39, 1476-1481.
35. Raut, E.R., Bedmohata, M.A., & Chaudhari, A.R., 2022. Comparative study of preparation and characterization of activated carbon obtained from sugarcane bagasse and rice husk by using H3PO4 and ZnCl2. Materials Today: Proceedings, 66, 1875-1884.
36. Saleh, T.A., 2021. Carbon nanotube-incorporated

alumina as a support for MoNi catalysts for the efficient hydrodesulfurization of thiophenes. Chemical Engineering Journal, 404, 126987.

37. Saleh, T.A., 2020. Characterization, determination and elimination technologies for sulfur from petroleum: Toward cleaner fuel and a safe environment. Trends in Environmental Analytical Chemistry, 25, e00080.
38. Saleh, T.A., Al-Hammadi, S.A., Tanimu, A., & Alhooshani, K., 2018. Ultra-deep adsorptive desulfurization of fuels on cobalt and molybdenum nanoparticles loaded on activated carbon derived from waste rubber. Journal of colloid and interface science, 513, 779-787.
39. Sarıcı-Özdemir, Ç., & Önal, Y., 2018. Synthesis of new activated carbons produced from polymer waste. Fullerenes, Nanotubes and Carbon Nanostructures, 26(7), 451-457.
40. Sadare, O. O., & Daramola, M.O., 2019. Adsorptive removal of dibenzothiophene from petroleum distillates using pomegranate leaf (Punica granatum) powder as a greener adsorbent. Chemical Engineering Communications, 206(3), 333-345.
41. Song, H., Wan, X., Dai, M., Zhang, J., Li, F.,& Song, H., 2013. Deep desulfurization of model gasoline by selective adsorption over Cu–Ce bimetal ion-exchanged Y zeolite. Fuel Process. Technol, 116, 52-62.
42. Shah, S.S., Ahmad, I.,& Ahmad, W.,2015. Adsorptive desulphurization study of liquid fuels using Tin (Sn) impregnated activated charcoal. Journal of hazardous materials 2016, 304, 205-213.
43. Tao, H.C., Zhang, H.R., Li, J.B., & Ding, W.Y., 2015. Biomass based activated carbon obtained from sludge and sugarcane bagasse for removing lead ion from wastewater. Bioresource technology, 192, 611-617.
44. Varila, T., Bergna, D., Lahti, R., Romar, H., Hu, T., & Lassi, U., 2017. Activated carbon production from peat using ZnCl2: Characterization and applications. BioResources, 12(4), 8078-8092.
45. Wang, F., Tang, X., Liu, Y., Qin, G., & Hu, Y., 2018. Preparation of activated carbon from eupatorium adenophorum for application in the desulfurization of model gasoline. Petroleum Science and Technology, 36(20), 1703-1709.
46. Wang, X., Wang, S., Yin, X., Chen, J., & Zhu, L., 2014. Activated carbon preparation from cassava residue using a two-step KOH activation: preparation, micropore structure and adsorption capacity. Journal of Biobased Materials and Bioenergy, 8(1), 35-42.
47. Wu, Q., Lv, X., Xu, N., Xin, L., Lin, G., Chen, K., & He, M. 2023. Upcycling plastic polymers into single-walled carbon nanotubes from a magnesia supported iron catalyst. Carbon, 215, 118492.
48. Xia, M., Shao, X., Sun, Z., & Xu, Z., 2020. Conversion of cotton textile wastes into porous carbons by chemical activation with ZnCl2, H3PO4, and FeCl3. Environmental Science and Pollution Research, 27, 25186-25196.
49. Xia, Y., Li, Y., Gu, Y., Jin, T., Yang, Q., Hu, J., & Wang, H., 2016. Adsorption desulfurization by hierarchical porous organic polymer of poly-methylbenzene with metal impregnation. Fuel, 170, 100-106.
50. Xiong, H., Xiao, Y., & Yan, Z., 2021. Preparation of activated carbon and its adsorption of naphthalene in liquid paraffin oil. Colloid and Interface Science Communications, 43, 100460.
51. Yaseen, M., Ullah, S., Ahmad, W., Subhan, S., & Subhan, F., 2021. Fabrication of Zn and Mn loaded activated carbon derived from corn cobs for the adsorptive desulfurization of model and real fuel oils. Fuel, 284, 119102.
52. Yağmur, H.K., & Kaya, İ., 2021. Synthesis and characterization of magnetic ZnCl2-activated carbon produced from coconut shell for the adsorption of methylene blue. Journal of molecular structure, 1232, 130071.
53. Zeng, F., Liao, X., Hu, H., & Liao, L., 2018. Effect of potassium hydroxide activation in the desulfurization process of activated carbon prepared by sewage sludge and corn straw. Journal of the Air & Waste Management Association, 68(3), 255-264.
54. Zhang, G., Yang, H., Jiang, M., & Zhang, Q., 2022. Preparation and characterization of activated carbon derived from deashing coal slime with ZnCl2 activation. Colloids and Surfaces A: Physicochemical and Engineering Aspects, 641, 128124.
55. Zu, Y., Guan, L., Guo, Z., Huang, C., He, D., & Mei, Y., 2021. Deep removal of thiophene and benzothiophene in low-sulfur fuels over the efficient CeAlSBA-15 adsorbent synthesized by sequential alumination and cerium incorporation. Chemical Engineering Journal, 416, 127984.